Received November 17, 2020, accepted December 2, 2020, date of publication December 7, 2020,
date of current version December 16, 2020.

Digital Object Identifier 10.1109/ACCESS.2020.3043053

OAM Mode Order Conversion and Clutter Rejection With OAM-Coded RFID Tags

MOHAMED HAJ HASSAN[1], BENEDIKT SIEVERT[1], (Member, IEEE), JAN TARO SVEJDA[1], (Member, IEEE), ALI ALHAJ ABBAS[2], (Member, IEEE), ALEJANDRO JIMÉNEZ-SÁEZ[3], (Member, IEEE), AYA MOSTAFA AHMAD[4], MARTIN SCHÜßLER[3], (Member, IEEE), ANDREAS RENNINGS[1], (Member, IEEE), KLAUS SOLBACH[2], (Member, IEEE), THOMAS KAISER[2], (Senior Member, IEEE), ROLF JAKOBY[3], (Member, IEEE), AYDIN SEZGIN[4], (Senior Member, IEEE), AND DANIEL ERNI[1], (Member, IEEE)

[1]General and Theoretical Electrical Engineering (ATE), Faculty of Engineering, CENIDE–Center for Nanointegration Duisburg-Essen, University of Duisburg-Essen, 47048 Duisburg, Germany
[2]Institute of Digital Signal Processing, University of Duisburg-Essen, 47048 Duisburg, Germany
[3]Institute of Microwave Engineering and Photonics, Technische Universität Darmstadt, 64283 Darmstadt, Germany
[4]Department of Electrical Engineering, Ruhr-Universität Bochum, 44801 Bochum, Germany

Corresponding author: Mohamed Haj Hassan (mohamed.haj-hassan@uni-due.de)

This work was supported in part by the Deutsche Forschungsgemeinschaft (DFG, German Research Foundation)—TRR 196MARIE in the framework of projects S03, S04, and C09, under Grant 287022738, and in part by the Open Access Publication Fund of the University of Duisburg-Essen.

ABSTRACT In this article, a uniform helically arranged dielectric resonator array can generate Orbital Angular Momentum waves (OAM) causing a conversion of OAM mode orders m from an incoming mode m_{in} to an outgoing mode m_{out}. The operating frequency is set as 10 GHz to facilitate the measuring process. This new approach provides additional OAM values per digit in the RFID technology according to the excited OAM modes $m_n \in \{\ldots, -2, -1, 0, 1, 2, \ldots\}$ instead of the conventional binary values $b_n \in \{0, 1\}$. Thus, more information content is revealed. Through the OAM concept, a $m_1 m_2$ 2-digits OAM coded tag is obtained upon the employment of two uniform helically arranged cylindrical dielectric resonator arrays operating at two different frequencies $f_1 = 10$ GHz, and $f_2 = 11$ GHz. Each array has 8 DRs but with different radius yielding a reduction of the mutual coupling between the varied circular arrays. The interaction between the phase delayed radiation of each DR element in the array generates different vortex waves with corresponding OAM mode orders. In order to achieve the correct phase delay, the elevation of each DR is specified by the desirable OAM mode order, the number of elements and the propagation wavelength. At first, the generation of OAM mode orders -1, 2, and -3 is carried out. Then, mode conversion from 0 to -1, $+1$ to -2, -1 to 0, $+2$ to -3, and -2 to $+1$ are depicted. After that, two simulated examples of 2-digits OAM coded tags with the code $\{-1, 1\}$ and $\{-2, 0\}$ are presented. A conversion of mode 0 to mode 1 has been simulated and also measured, where an additional metal sheet is used to evaluate the distortion in the OAM modes. As a result, this study demonstrates that the uniform helically arranged DR arrays can convert the incoming OAM mode order into another one, where the clutter from broadside direction is rejected due to the Butler matrix (BM), which interferes the clutter destructively.

INDEX TERMS Orbital angular momentum OAM, vortex waves, spiral waves, OAM mode conversion, OAM lens, dielectric resonator, clutter rejection, RFID tags, passive chipless RFID.

I. INTRODUCTION

Radio Frequency Identification Technology (RFID) offers a solution to the issue of the difficult distinction and identification of many articles where it can detect, locate, identify and track these items using radio waves. An RFID system consists of an RFID reader and a transponder device (radio receiver and transmitter). When an electromagnetic (EM) interrogation pulse ejected from a nearby RFID reader triggers the transponder part, it responds back and

The associate editor coordinating the review of this manuscript and approving it for publication was Chinmoy Saha.

sends out signals that are characterized by a specific code known to the reader. Furthermore, there are two kinds of RFID tags, namely passive and active. The active tags require an extra battery power to operate, as opposed to the passive tags which are powered by the electromagnetic field via the RFID reader having much lower production costs [1]. In addition, the passive dielectric resonators (DRs) designed in this study are composed of a dielectric material with a high permittivity. At certain resonance frequencies and corresponding EM field distribution (modes) which correspond to the eigen-frequencies, the passive DR shows the largest radar cross section (RCS). The corresponding quality factor and the mode's operating frequency depend mainly on the relative permittivity, the size and the loss tangent ($\tan\delta$) of the DR [2]. By illuminating a conventional RFID tag (1-bit tag) with plane waves, the backscattered signal may contain information in form of a sensed value [3]–[5] or frequency identification [6]. The modes of a DR can be frequency shifted by altering the dimensions of the DR. Through this manner, an N-digit coded tag can be formed with N differently sized DRs. Nevertheless, the number of digits is limited by the spectral mode spacing between the two adjacent modes thus avoiding the distortion between the different DRs resonating at different frequencies [7].

Electro-magnetic (EM) waves can carry an angular momentum, which can be divided into a spin angular momentum and an orbital angular momentum (OAM) in paraxial beams. The spin angular momentum is well known as the circular polarization that describes the intrinsic property of the spin characteristics of the EM rotational degrees of freedom. In contrast, the OAM of the EM wave is an extrinsic property that describes the orbital characteristics of its rotational degrees of freedom, which has a helical transverse phase structure of $\exp(-j\varphi m)$, where φ is the transverse azimuthal angle and m is an unbounded integer that indicates the OAM mode order [8]. Containing an infinite number of mutually orthogonal states m (i.e. the OAM mode order), the OAM waves present a new degree of freedom in signal coding, enabling a new spatial division multiplexing (SDM) procedure scheme with independent data streams at the same operating frequency [9]. Hence, an improvement of both capacity and spectral efficiency could be gained. The OAM mode division multiplexing (OAM-MDM) is a new physical transmission technology which can also be used in combination with the other multiplexing methods (time, frequency, polarization and code) yielding an enormous improvement in data transmission [10]. The OAM waves are characterized by a doughnut-shaped radiation pattern with the helical phase front and with a singularity, where the zero is centered in the doughnut-shaped radiation pattern. Concerning the generation of vortex waves, there are many available ways such as metasurfaces [11], spiral phase plates (SPP) [12], holographic plates (HP) [13], elliptical patch antennas which excite two at the same time orthogonally oriented resonant mode patterns [14], [15], reflectors [16] or uniform circular patch arrays (UCA) [17]. However, these approaches do not discuss the limitations compared to MIMO systems [18]. Furthermore, the vortex waves are advantageous for the field of imaging [19] and particularly for spinning objects, which can still be used even when the line of sight (LOS) is orthogonal to the object [20]. By means of tailored phased-array antenna concepts [21], the OAM beam is steered in which the typically large beam divergence inherent to the vortex waves can be reduced upon the usage of a lens [22]–[24], or a reflector [16], [25], [26].

In this work, not only the zeroth mode order is converted, but the rest of the modes also undergo certain conversion as introduced presenting its novelty. The initial idea is proposed in [27], whose RFID codes are increased by means of helically arranged DRs arrays in addition to the novelty of the clutter rejection's possibility. In contrast, the conventional arrangement of DRs suffers from the strong clutter leading to a loss in the transmitted data. This article is classified into the following sections. At first, Section II reveals the reflection coefficient and the far-field radiation pattern of a rectangular patch antenna in addition to the transmission coefficient of a cylindrical dielectric resonator. Then, the radiation pattern and the phase front of the converted OAM mode are depicted in proceeding Section III. Followed by Section IV, where the concept of N-digits coded tag enabling OAM coding of frequency tags with two digits with values $\{-3, -2, -1, 0, 1, 2, 3\}$ according to the realized OAM mode order. Furthermore, in Section V, the measured transmission coefficient of an eight cylindrical dielectric resonator array with and without a metal plate is introduced. Finally, Section VI is presented as a conclusion of this study.

II. DESIGN OF RECTANGULAR PATCH ANTENNA AND CYLINDRICAL DIELECTRIC RESONATOR

With the aid of the MoM-solver FEKO, a rectangular patch antenna operating at 10 GHz is simulated to simplify the experimental studies. This y-polarized patch antenna is designed on a Rogers RO4003C substrate with a relative permittivity of 3.55 and a height of 1.524 mm. While the simulated patch antenna is specified by 7.53 mm length (about $\lambda_{\text{eff}}/2$) and 10.8 mm width. In Fig. 1 (a, b, and c), the patch antenna and its radiation pattern are illustrated in 2D and 3D. When the directional antenna is matched to 50 Ω, the gain is maximized through avoiding reflections at the antenna port hence yielding a gain of about 6.1 dBi (Fig. 1 (c)). Moreover, the simulated return loss S_{11} is about -28 dB unlike the measured one which is about -12.7 dB at the operating frequency of 10 GHz (Fig. 1 (d)). This is due to the changing of the antenna's characteristic impedance causing more reflections and a shift of the resonance frequency to 10.2 GHz. The underlying printed circuit board (PCB) board is characterized by a size of 30 mm × 30 mm. A cylindrical dielectric resonator reacts and resonates once illuminated by incident plane waves. This DR supports three kinds of mode (Transverse Electric (TE), Transverse Magnetic (TM) and Hybrid Modes (HE)) whose eigen frequency and corresponding quality factor depend mainly on the relative permittivity

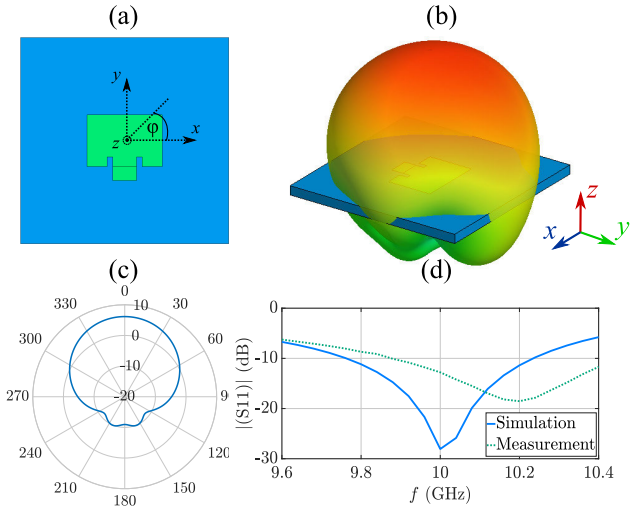

FIGURE 1. The top view of rectangular patch antenna (a), the simulated radiation pattern (dBi) in 3D at 10 GHz (b), the simulated radiation pattern (dBi) in 2D at $\varphi = 0°$ (*H*-plane) (c), and the return loss S_{11} (d).

ε_r, the size, the loss tangent (tanδ), and on the orientation of the DR. To be more specific, the 10 GHz operated DR has a 3.2 mm radius, a 3 mm height, and a relative permittivity $\varepsilon_r = 37$ (ceramic) thus leading the DR to radiate with the mode HE_{11}. In Fig. 2 (a, and b), the simulated and measured setup is shown with a separation of about 100 mm between the two horn antennas on one hand and between the horn antennas and the DR on the other hand. In Fig. 2 (c), the simulated and the measured insertion loss S_{21} of the two horn antennas including and excluding DR are presented within 9.6 GHz and 10.4 GHz. However, an increased S_{21} of about 5 dB appears specifically between 10 GHz and 10.3 GHz indicating the presence of the DR. The measured S_{21} is in good agreement with the full-wave MoM simulation calculated with Feko.

III. OAM MODE CONVERSION

The cylindrical DR mentioned in the previous section is used to form a helically arranged cylindrical DR array in order to re-radiate vortex waves once illuminated by an antenna. These helically arranged DR array radiates into two opposite directions (forward and backward) based on the asymmetric doughnut radiation pattern of each DR. The forward transmitted OAM mode order propagates in the same direction of the incident OAM mode order thus having the same OAM mode order m_{in}. Whereas, the backward reflected OAM mode order propagates in the opposite direction of the incident OAM mode order thus having a different OAM mode order m_{out} depending on the DRs arrangement. The phase shift between each pair of the adjacent DRs, which is essential to OAM waves, is defined by the following equation:

$$\Delta\varphi = \frac{2\pi m}{N}, \tag{1}$$

where N is the number of single DR, and m is the mode order of the vortex waves. Thus, the height h

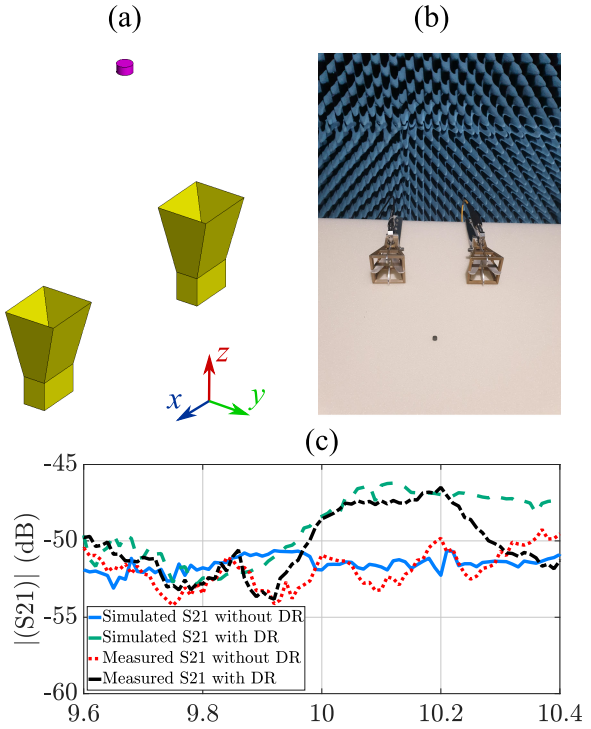

FIGURE 2. The simulation setup of the cylindrical DR (a), the measurement setup of the cylindrical DR in an anechoic chamber (b), and the simulated and measured S_{21} (dB) of two standard gain horn antennas without and with DR from 9.6 GHz till 10.4 GHz.

(cf. Fig. 3 (a, b, and c)) between each azimuthally adjacent DR, due to the twofold path length of the electromagnetic waves, is determined by

$$h = \frac{m\lambda}{2N}. \tag{2}$$

If the DRs exceed the phase shift of 2π, the pitch p (cf. Fig. 3 (a, b, and c)), which is the total height between the lowest and the highest DR, can be shifted vertically downwards by $\lambda/2$ along the propagation-axis. In Fig. 3 (a, b, and c), three helically arranged cylindrical DRs array with three different OAM mode orders -1, $+2$, and -3 are illuminated by a rectangular patch antenna operating at 10 GHz, providing an incident OAM mode order of 0. Please note, that the different colors of the DRs are only to simplify the understand of the concept. Regarding equation (2), the height h between the adjacent DRs are 1.875 mm, 3.75 mm, and 5.625 mm with respect to the OAM mode orders -1, $+2$, and -3, respectively. The highest gain values of the backscattered direction of the DRs concerning the modes -1, $+2$, and -3 (cf. Fig. 3 (d)) are -17 dBi, -15.2 dBi, and -14.3 dBi at 154°, 154°, and 219°, respectively. Note that the diagram actually does not depict true side lobes but rather cross sections of doughnut shaped radiation patterns. In addition, the orders of the backscattered OAM mode depend on the quantity of DRs, on the incident OAM mode order and on the spacing between each pair of adjacent DRs. Fig. 3 (e, f, and g) shows the conversion of the zeroth OAM

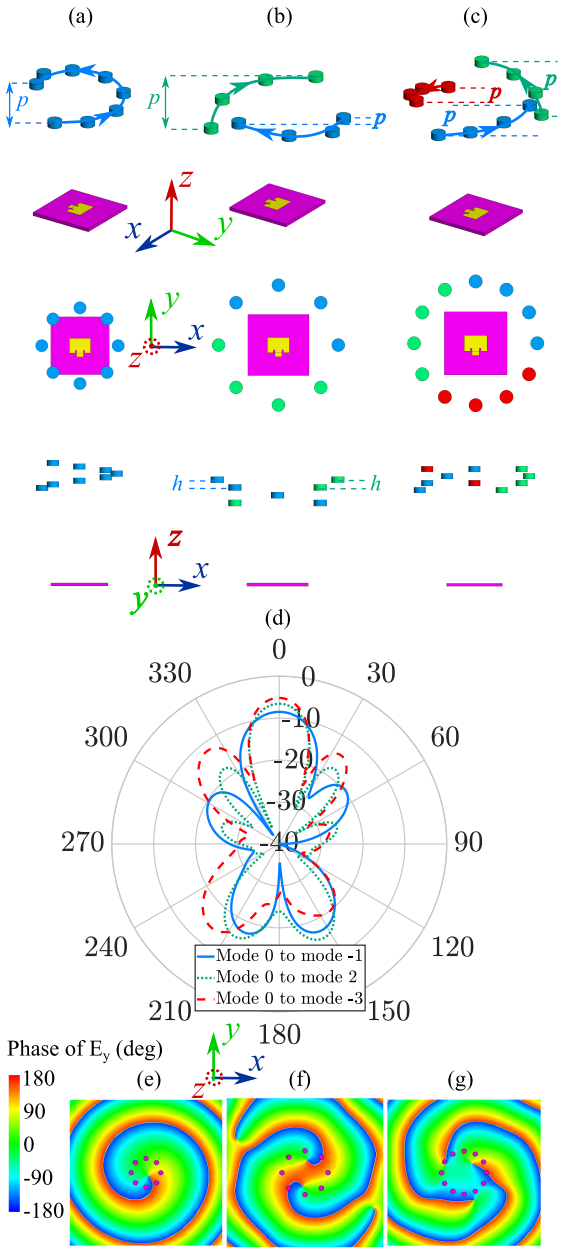

FIGURE 3. The generation of OAM mode orders −1, +2 and −3 (a, b, and c), the simulated radiation pattern (dBi) in 2D at $\varphi = 0°$ (*H*-plane) for the OAM mode orders −1, +2 and −3 at 10 GHz (d), and the simulated phase distribution ($x = -100$ till 100 mm, $y = -100$ till 100 mm, $z = 200$ mm) at 10 GHz for the OAM mode orders −1 (e), +2 (f), and −3 (g).

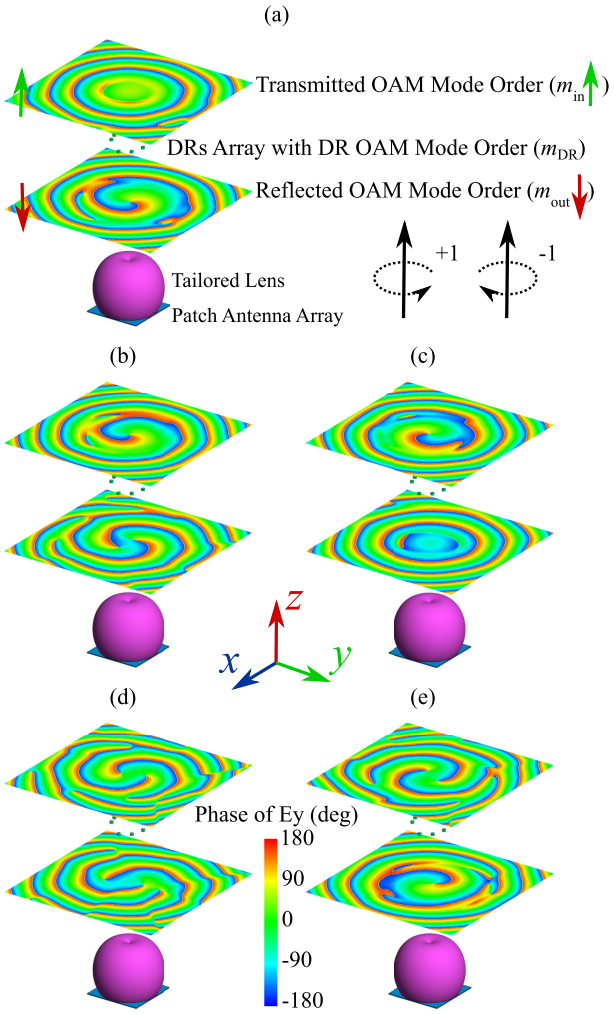

FIGURE 4. The different simulated scenarios for the OAM mode order conversion at an OAM coded tag with $m_{DR} = +1$ from the incident OAM mode order m_{in} to the reflected OAM mode order m_{out} showing reflected and transmitted beams only: 0 to −1 (a), +1 to −2 (b), −1 to 0 (c), +2 to −3 (distorted) (d), and −2 to +1 (e).

mode order into the OAM mode orders of −1, 2, and −3, respectively, where the phase distribution is a distribution of one helix, two helices and three helices. Further, the positive OAM modes are specified by the right-handed thread whereby the rotation of the vortex waves is clockwise, in contrary to the negative OAM modes that rotate counterclockwise. Moving to Fig. 4, the conversion of vortex beams from different OAM mode orders [0 (a), +1 (b), −1 (c), +2 (d), and −2 (e)] is demonstrated. A lensed patch antenna array [22] emits towards the structured target that is configured according to the OAM mode order +1. The lens is crucial for the beam divergence compensation otherwise the OAM mode conversion will not be performed well. In case (a), the OAM mode order 0 is transmitted and converted to OAM mode −1. While the cases (b) and (c) undergo OAM mode orders +1 and −1 conversion into the mode orders −2 and 0, respectively. Similar to the previous cases, the cases (d) and (e) transmit the mode orders +2 and −2 and convert them into the OAM mode orders −3 and +1. Moreover, the converted mode order m_{out} is equal to the opposite sign of the sum of the incident OAM mode order m_{in} and the DRs OAM mode order m_{DR}.

$$m_{out} = -(m_{in} + m_{DR}). \tag{3}$$

However, the case (d) with the +2 mode exhibits slight distortion because of the strong divergence of the doughnut-shaped OAM beam with the mode order 2. In Fig. 4, all of the 5 cases are displayed with the forward (transmitted) and backward

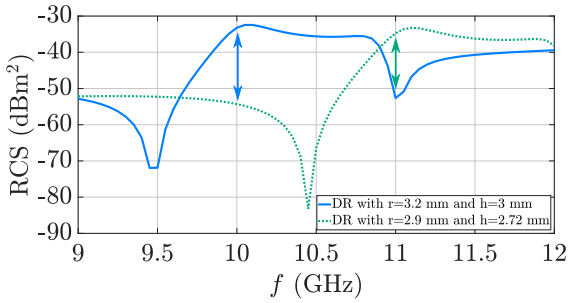

FIGURE 5. The simulated radar cross section (RCS) (dBm^2) for two different DRs with two different radii and heights from 9 GHz to 12 GHz.

(reflected) scattered beam without taking into account the strong beam of the UCA antennas for reason of clarity.

IV. N-DIGITS CODED TAG

Converting the OAM mode order from mode 0 (plane waves) to another mode may have a new advantage with respect to the application of RFID. The conventional RFID application is based on the illumination of the DR with plane waves where the backscattered signal carries information in the form of frequency identification or a sensed value. The DR element's absence leads to understanding the value of 0, and its presence leads to understanding the value of 1. Upon the usage of N different DR elements in one tag, the number of codes increase to 2^N in which each DR is operating at a different frequency. However, the high demand of labeled products is greater than the limited capacity of the number of codes which encourages the search for new methods to increase the number of tags/codes. Two different cylindrical DRs with different radii and heights are simulated to operate at 10 GHz, and 11 GHz separately. The first DR is characterized with radius and height of 3.2 mm/3 mm value, while the second one 2.9 mm/2.72 mm. In Fig. 5, the radar cross section (RCS) of the two DRs is illustrated from 9 GHz to 12 GHz in which the maximum RCS is shown to be about -32 dBm^2. In addition, the difference between the DRs is about 20 dB which is enough to reduce the interference between the different DRs. The same helically DRs arrangement is applied as in Section (III) so that a 2-digits OAM coded tag is formed (cf. Fig. 6). A desirable enhancement of the isolation between the two helically arranged dielectric resonator arrays is accomplished through the usage of different radii for each helix. To be more specific, 20 mm, and 30 mm radii are applied for the frequencies 11 GHz, and 10 GHz, respectively. As noted, upon the usage of the same or closer frequencies, the sequence of codes is missing in a way that the receiver can not anymore distinguish between the codes, e.g. 12 or 21. Therefore, many codes become absent due to redundancy. The maximum number of values per digit D in one circular array is based on the number of the DRs N, which determines the number of possible mode orders [27]. This is defined by

$$D = 2 \cdot \lfloor (\frac{N-1}{2}) \rfloor + 1. \quad (4)$$

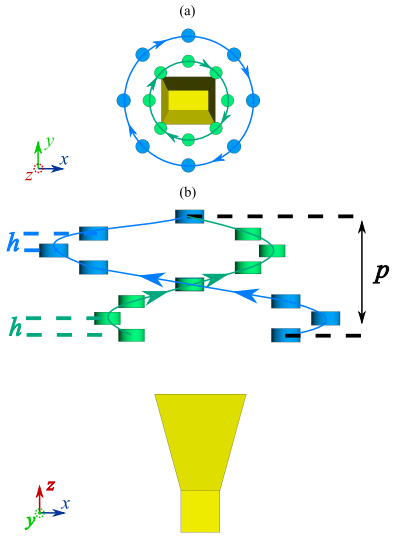

FIGURE 6. Two helically arranged DR arrays of 2 × 8 (Top and Side view).

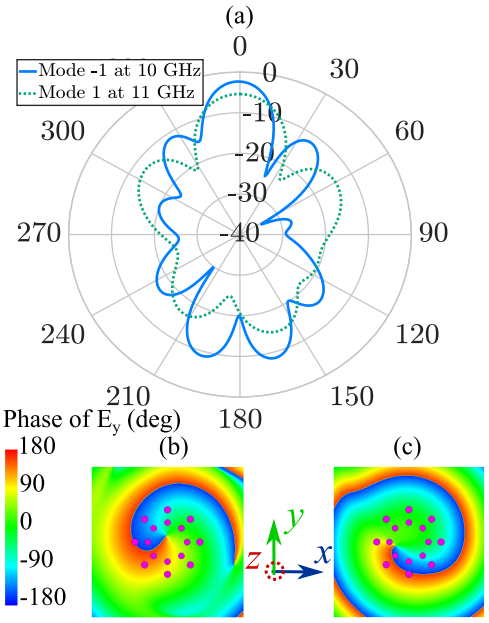

FIGURE 7. The simulated radiation pattern (dBi) in 2D at $\varphi = 0°$ (H-plane) for the 2-digits OAM coded tag {−1, 1} at 10 GHz, and 11 GHz (a), and the simulated phase distribution ($x = -100$ till 100 mm, $y = -100$ till 100 mm, $z = 200$ mm) at 10 GHz for $m = -1$ (b), and 11 GHz for $m = 1$ (c).

Adding +1 in (4) considers the zeroth mode order, which can be reached if the pitch is zero. A helically arranged DR array composed of 8 elements can provide $D = 7$ values per digit $\{-3, -2, -1, 0, 1, 2, 3\}$. So, the equation (4) generates $D^k = 49$ OAM codes in case of $k = 2$ and $D = 7$, where k is the number of DR helical arrays. While for $k = 3$ and $D = 7$, the number of codes will be increased to 343 codes, so it is better to use a spherical DR due to the more equidistant resonance frequencies. The initial idea has been presented in [27], where two examples {−1,1,0} and {−2,1,0} of 3-digits OAM-coded RFID Tags have been carried out by the aid of spherical dielectric resonator arrays. In Figs. 7 and 8 (a), the simulated radiation pattern of the

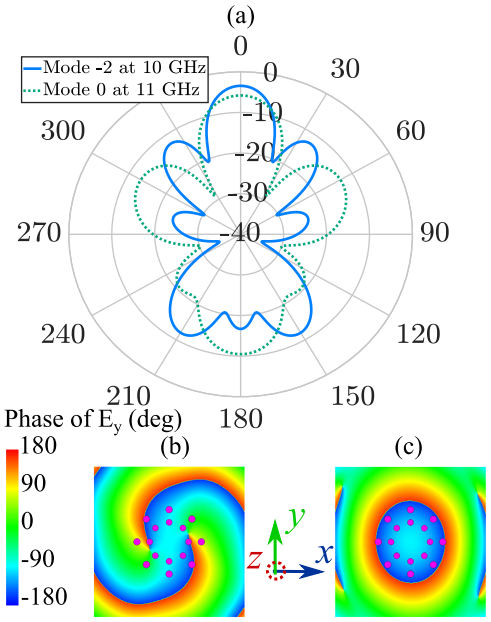

FIGURE 8. The simulated radiation pattern (dBi) in 2D at $\varphi = 0°$ (H-plane) for the 2-digits OAM coded tag $\{-2, 0\}$ at 10 GHz, and 11 GHz (a), and the simulated phase distribution ($x = -100$ till 100 mm, $y = -100$ till 100 mm, $z = 200$ mm) at 10 GHz for $m = -2$ (b), and 11 GHz for $m = 0$ (c).

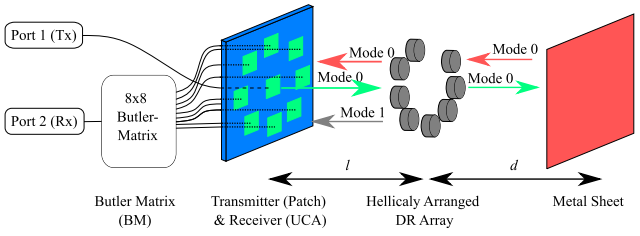

FIGURE 9. The schematic view of the measurement setup between a patch antenna, a helically arrangend DR array, and a metal sheet.

2-digits OAM coded tags $\{-1, 1\}$ and $\{-2, 0\}$ are displayed. The simulated phase distribution is presented at two different frequencies in Figs. 7 and 8 (b, and c). The digit 0 corresponds to the OAM mode order 0, which shows a constant phase distribution corresponding to the digit 1 in the conventional RFID tags. These two examples confirm the validity of the increasing RFID codes.

V. MEASUREMENT

In order to avoid undesirable reflections and distortions, the measurement is carried out in an anechoic chamber. A vector network analayzer (VNA) ZVA 40 from Rohde & Schwarz is utilized and calibrated with coaxial cables between 9 GHz till 11 GHz with 201 points. A transmit patch antenna is mounted in the middle of the UCA. The UCA task is to receive the reflected signal from the helically arranged DRs (cf. Figs. 9 and 10). The UCA has a radius of about 40 mm, so that the transmitting antenna can be placed easily. Variable receiving OAM mode orders are provided by a 8×8 Butler matrix (BM) which operates at 10 GHz and is connected to

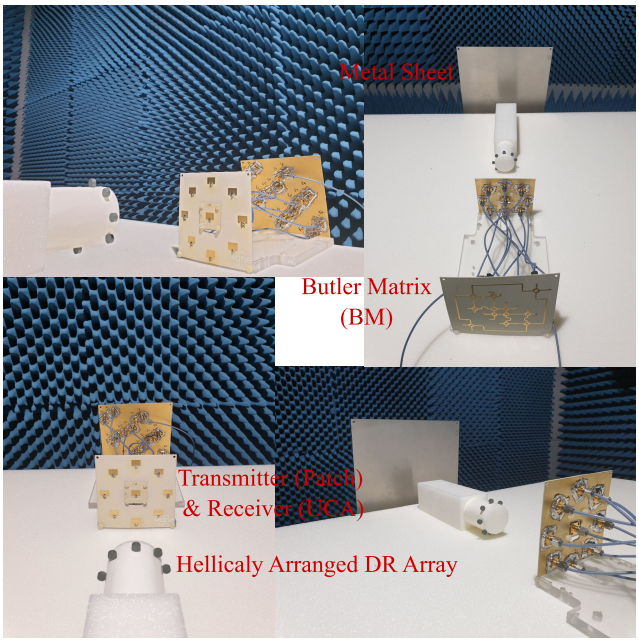

FIGURE 10. The measurement setup of patch antenna, UCA, BM and DRs in an anechoic chamber.

the UCA by eight coaxial cables of identical length (200 mm). Further, the whole system is suspended on a large piece of Rohacell with a permittivity of almost 1 in purpose to prevent the distortion and other undesirable side effects. Otherwise, the measurements would be manipulated if permittivity is higher. As a start, in Fig. 11 (a), the simulated and measured S_{21} between the patch antenna and the UCA representing the mutual coupling, non-ideality of the BM, and reflections from the room are presented and taken as reference for the next scenarios yielding a transmission of -58.3 dB for simulation and -51.85 dB for measurement at 10 GHz. Moving on to Fig. 11 (b), the simulated and the measured S_{21} with the existence of the helically arranged DRs assembled on cylindrical Rohacell is depicted, where the distance between each pair of adjacent DRs is about 15 mm ($\lambda/2$) in purpose to achieve the highest gain towards the UCA. The height h of the helically arranged DRs, which consist of 8 DRs, is adjusted according to equation (2) in order to convert the zeroth OAM mode order into the first OAM mode order. Consequently, the pitch equals seven times the height h, hence the pitch value of 13.125 mm. Due to the OAM divergence, the helically arranged DRs are separated from the UCA for a short distance, which is $l = 100$ mm. Increasing the number of the DRs can solve this divergence issue, and so can a lens. Very good agreement is shown between the simulated and the measured S_{21} on one side and about a 20 dB gain enhancement at 10 GHz compared to the case without DRs on the other side. The gain enhancement starts from 9.6 GHz up to about 11 GHz, because the DRs work well within this bandwidth. In Fig. 11 (c, d, and e), the same configuration is applied but with a metal sheet for three varied distances d of 300 mm, 400 mm, and 500 mm, in order to reveal the

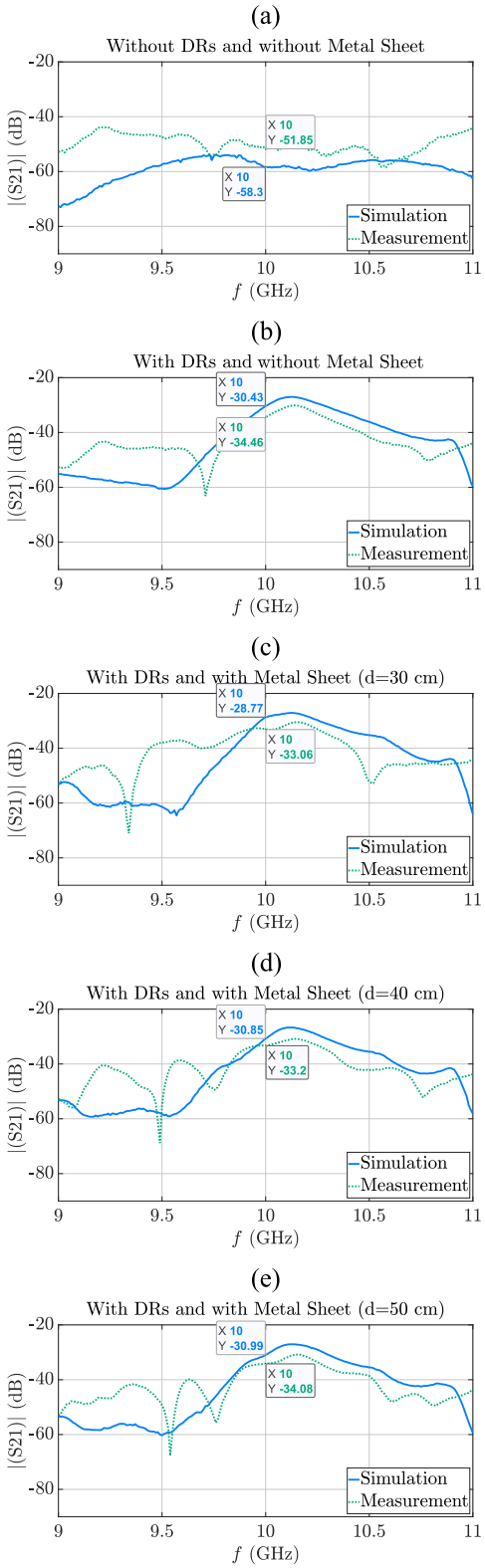

FIGURE 11. The simulated and measured S_{21} (dB) between the rectangular patch antenna and the UCA without DRs and without metal sheet (a), with DRs and without metal sheet (b), with DRs and with metal sheet for a distance d of 30 cm (c), 40 cm (d), and 50 cm (e).

influence as well as the distortion of a metal sheet on the S_{21}. The S_{21} results at 10 GHz show that the metal sheet has almost no effect on the transmission with the presence

TABLE 1. The insertion loss S_{21} (dB) for the five scenarios for the first OAM mode order at 10 GHz.

		Transmission S21 (dB)	
		Sim.	Meas.
		Without DRs	
Without metal sheet		-58.3	-51.85
		With DRs	
Without metal sheet		-30.43	-34.46
With Metal Sheet	d =30 cm	-28.77	-33.06
	d =40 cm	-30.85	-33.2
	d =50 cm	-30.99	-34.08

of the helically arranged DRs announcing a novel method to reject the clutter with the exception of the zeroth mode order. Such clutter rejection belonging to the BM is caused by different phase shifts resulting in destructive interference for the clutter, but constructive interference for the DR-coded OAM-signal. Table 1 summarizes the S_{21} at 10 GHz according to the five different scenarios. One can notice, there are some notches in the measurement results, particularly two fixed notches and one movable notch. The two fixed notches (about 9.7 GHz, and 10.6 GHz) appear due to the mutual coupling between the transmitter and the receiver (UCA). While, the moving notch occurs as a result of the following issues. At first, the patch antenna is not accurately positioned in the middle of the UCA as well as the height between the DRs is not exactly accurate resulting in a non-ideal phase shift between the DRs. Then, the BM has shown phase shift errors of about $\pm 5^{\circ}$. Moreover, the distance between the DRs and the antennas is neither exactly 100 mm nor accurately oriented with the antennas. Finally, the metal sheet is not precisely parallel to the antennas. However, the measurement is well accomplished and agrees well with the simulation, noting that this clutter rejection works well, if the interferer is orthogonal to the main beam direction.

VI. CONCLUSION

In this article, a new approach concerning the generation and conversion of OAM mode orders through helically arranged cylindrical dielectric resonator arrays is introduced. The interaction of the phase delayed radiation of each DR element in the array submits different vortex wave modes. However, the proposed tag design is scalable to operate in the mm-wave/THz range yielding smaller structures with low radar cross-sections (RCS). This RCS can be mitigated with the aid of a larger number of DRs. Furthermore, the RFID tag technology can provide larger codes with new multi-valued digits instead of the two conventional binary codings (0 and 1). Three mode orders -1, 2 and -3 are exemplarity converted from the zeroth OAM mode order. Moreover, the OAM mode order conversions of 0 to -1, $+1$ to -2, -1 to 0, $+2$ to -3, and -2 to $+1$ are presented. Two examples of 2-digits OAM coded tags with the code $\{-1, 1\}$ and $\{-2, 0\}$ have been simulated. Furthermore, the simulated

and measured S_{21} of the mode conversion 0 to 1 are in good agreement demonstrating the very low efficacy and distortion of an orthogonal metal sheet on the receiving OAM antenna due to the different phase shifts in the Butler matrix. This article has shown that the OAM waves are very useful for the RFID application by increasing the RFID codes and by rejecting the clutter from broadside direction.

REFERENCES

[1] S. Preradovic and N. Karmakar, "Chipless RFID: Bar code of the future," *IEEE Microw. Mag.*, vol. 11, no. 7, pp. 87–97, Dec. 2010.
[2] A. A. Abbas, M. El-Absi, A. Abuelhaijay, K. Solbach, and T. Kaiser, "THz passive RFID tag based on dielectric resonator linear array," in *Proc. 2nd Int. Workshop Mobile THz Syst. (IWMTS)*, Bad Neuenahr, Germany, Jul. 2019, pp. 1–5.
[3] A. J. Sáez, E. Polat, C. Mandel, M. Schüßler, B. Kubina, T. Scherer, N. Lautenschläger, and R. Jakoby, "Chipless wireless temperature sensor for machine tools based on a dielectric ring resonator," *Procedia Eng.*, vol. 168, pp. 1231–1236, Jan. 2016.
[4] B. Kubina, M. Schusler, C. Mandel, A. Mehmood, and R. Jakoby, "Wireless high-temperature sensing with a chipless tag based on a dielectric resonator antenna," in *Proc. IEEE SENSORS*, Baltimore, MD, USA, Nov. 2013, pp. 1–4.
[5] D. J. Thomson, D. Card, and G. E. Bridges, "RF cavity passive wireless sensors with time-domain gating-based interrogation for SHM of civil structures," *IEEE Sensors J.*, vol. 9, no. 11, pp. 1430–1438, Nov. 2009.
[6] A. Jiménez-Sáez, M. Schüßler, D. Pandel, N. Benson, and R. Jakoby, "3D printed 90 GHz frequency-coded chipless wireless RFID tag," in *Proc. IEEE MTT-S Int. Microw. Workshop Ser. Adv. Mater. Processes RF THz Appl. (IMWS-AMP)*, Bochum, Germany, Jul. 2019, pp. 4–6.
[7] M. El-Absi, A. A. Abbas, A. Abuelhaija, F. Zheng, K. Solbach, and T. Kaiser, "High-accuracy indoor localization based on chipless RFID systems at THz band," *IEEE Access*, vol. 6, pp. 54355–54368, 2018.
[8] C. Zhang and L. Ma, "Millimetre wave with rotational orbital angular momentum," *Sci. Rep.*, vol. 6, no. 1, pp. 1–8, Sep. 2016.
[9] J. Yang, H. Liu, J. Wen, F. Pang, N. Chen, Z. Chen, and T. Wang, "Excitation and transmission of 12 OAM modes in 3.7-km-long ring fiber with high refractive index difference," in *Proc. Asia Commun. Photon. Conf. (ACP)*, Hangzhou, China, Oct. 2018, pp. 1–4.
[10] W. Zhang, S. Zheng, X. Hui, R. Dong, X. Jin, H. Chi, and X. Zhang, "Mode division multiplexing communication using microwave orbital angular momentum: An experimental study," *IEEE Trans. Wireless Commun.*, vol. 16, no. 2, pp. 1308–1318, Feb. 2017.
[11] F. Qin, L. Wan, L. Li, H. Zhang, G. Wei, and S. Gao, "A transmission metasurface for generating OAM beams," *IEEE Antennas Wireless Propag. Lett.*, vol. 17, no. 10, pp. 1793–1796, Oct. 2018.
[12] P. Schemmel, G. Pisano, and B. Maffei, "Modular spiral phase plate design for orbital angular momentum generation at millimetre wavelengths," *Opt. Exp.*, vol. 22, no. 12, pp. 14712–14726, 2014.
[13] F. E. Mahmouli and S. D. Walker, "4-Gbps uncompressed video transmission over a 60-GHz orbital angular momentum wireless channel," *IEEE Wireless Commun. Lett.*, vol. 2, no. 2, pp. 223–226, Apr. 2013.
[14] J. J. Chen, Q. N. Lu, F. F. Dong, J. J. Yang, and M. Huang, "Wireless oam transmission system based on elliptical microstrip patch antenna," *Opt. Exp.*, vol. 24, no. 11, pp. 11531–11538, 2016.
[15] M. Barbuto, M.-A. Miri, A. Alú, F. Bilotti, and A. Toscano, "A topological design tool for the synthesis of antenna radiation patterns," *IEEE Trans. Antennas Propag.*, vol. 68, no. 3, pp. 1851–1859, Mar. 2020.
[16] T. Nguyen, R. Zenkyu, M. Hirabe, T. Maru, and E. Sasaki, "A study of orbital angular momentum generated by parabolic reflector with circular array feed," in *Proc. Int. Symp. Antennas Propag. (ISAP)*, Okinawa, Japan, 2016, pp. 708–709.
[17] Q. Bai, A. Tennant, B. Allen, and M. U. Rehman, "Generation of orbital angular momentum (OAM) radio beams with phased patch array," in *Proc. Loughborough Antennas Propag. Conf. (LAPC)*, Loughborough, U.K., Nov. 2013, pp. 410–413.
[18] A. F. Morabito, L. Di Donato, and T. Isernia, "Orbital angular momentum antennas: Understanding actual possibilities through the aperture antennas theory," *IEEE Antennas Propag. Mag.*, vol. 60, no. 2, pp. 59–67, Apr. 2018.
[19] J. Wang, K. Liu, Y. Cheng, and H. Wang, "Vortex SAR imaging method based on OAM beams design," *IEEE Sensors J.*, vol. 19, no. 24, pp. 11873–11879, Dec. 2019.
[20] K. Liu, X. Li, Y. Gao, H. Wang, and Y. Cheng, "Microwave imaging of spinning object using orbital angular momentum," *J. Appl. Phys.*, vol. 122, no. 12, Sep. 2017, Art. no. 124903.
[21] M. Haj Hassan, M. Al-Mulla, B. Sievert, A. Rennings, and D. Erni, "Evaluation of different phased array approaches for orbital angular momentum beam steering," in *Proc. 13th German Microw. Conf. (GeMiC)*, Cottbus, Germany, 2020, pp. 1–4.
[22] M. H. Hassan, B. Sievert, A. Rennings, and D. Erni, "Reducing the divergence of vortex waves with a lens tailored to the utilized circular antenna array," in *Proc. 2nd Int. Workshop Mobile THz Syst. (IWMTS)*, Bad Neuenahr, Germany, Jul. 2019, pp. 1–4.
[23] H. Fukumoto, H. Sasaki, D. Lee, and T. Nakagawa, "Beam divergence reduction using dielectric lens for orbital angular momentum wireless communications," in *Proc. Int. Symp. Antennas Propag. (ISAP)*, Okinawa, Japan, 2016, pp. 680–681.
[24] Y. Yao, X. Liang, W. Zhu, J. Li, J. Geng, R. Jin, and K. Zhuang, "Realizing orbital angular momentum (OAM) beam with small divergence angle by Luneberg lens," in *Proc. IEEE Int. Symp. Antennas Propag. USNC/URSI Nat. Radio Sci. Meeting*, San Diego, CA, USA, Jul. 2017, pp. 367–368.
[25] J. Y. Hong, W. Lee, B.-S. Kim, M.-S. Kang, J.-B. Kim, W. J. Byun, and M. S. Song, "Use of tractroid factor in deformed parabolic reflector antenna which transfers orbital angular momentum modes," in *Proc. Int. Conf. Inf. Commun. Technol. Converg. (ICTC)*, Jeju, South Korea, Oct. 2017, pp. 1229–1231.
[26] F. Qin, J. Yi, W. Cheng, Y. Liu, H. Zhang, and S. Gao, "A high-gain shared-aperture dual-band OAM antenna with parabolic reflector," in *Proc. 12th Eur. Conf. Antennas Propag. (EuCAP)*, London, U.K., 2018, pp. 1–4.
[27] M. H. Hassan, A. A. Abbas, A. Jiménez-Sáez, A. M. B. Sievert, M. Schüßler, A. Rennings, K. Solbach, T. Kaiser, R. Jakoby, A. Sezgin, and D. Erni, "Passive orbital angular momentum RFID tag based on dielectric resonator arrays," in *Proc. 3nd Int. Workshop Mobile THz Syst. (IWMTS)*, Essen, Germany, 2020, pp. 1–4.

MOHAMED HAJ HASSAN was born in Beirut, Lebanon. He received the B.Sc. degree in electrical engineering and the M.Sc. degree in high-frequency technology from the Technical University of Berlin, Berlin, Germany, in 2010 and 2012, respectively. He worked as an RF specialist in the industry for about two years. From 2015 to 2017, he was with the Technical University of Ilmenau, Ilmenau, Germany, in the field of Ground Penetration Radar GPR. Since 2017, he has a member of the Laboratory of General and Theoretical Electrical Engineering, University of Duisburg-Essen. His research interests include RF and antenna technology, mm-waves, vortex waves, electromagnetic metamaterials, and computational electromagnetics.

BENEDIKT SIEVERT (Member, IEEE) was born in Krefeld, Germany. He received the B.Sc. degree in electrical engineering and the M.Sc. degree in high-frequency systems from the University of Duisburg-Essen in 2017 and 2019, respectively. Since 2017, he has been a member of the Laboratory of General and Theoretical Electrical Engineering, University of Duisburg-Essen. His research interests include mm-wave on-chip antennas, electromagnetic metamaterials, theoretical, and computational electromagnetics.

JAN TARO SVEJDA (Member, IEEE) received the B.Sc. degree in electrical engineering from the University of Applied Science, Düsseldorf, Germany, in 2008, and the M.Sc. and Dr.-Ing. degrees in electrical engineering and information technology from the University of Duisburg-Essen, Duisburg, Germany, in 2013 and 2019, respectively. His Dr.-Ing. research work was on the field of X-nuclei-based magnetic resonance imaging. He is currently a Research Assistant with the Department of General and Theoretical Electrical Engineering, University of Duisburg-Essen, where he is involved in teaching several lectures and courses mainly in the field of electrical engineering. His general research interest includes all aspects of theoretical and applied electromagnetics, with an emphasis on medical applications, electromagnetic metamaterials, and scientific computing methods.

ALI ALHAJ ABBAS (Member, IEEE) received the B.Sc. degree in electrical/communication engineering from Yarmouk University, Irbid, Jordan, in 2010, and the M.Sc. degree from the University of Jordan, Amman, Jordan, in 2016. He is currently pursuing the Ph.D. degree with the Institute of Digital Signal Processing, University of Duisburg-Essen. From 2011 to 2017, he was a Teaching Assistant and a Lecturer with Applied Science Private University, Jordan. He is currently a Research Fellow with the Collaborative Research Center for the Project Mobile Material Characterization and Localization by Electromagnetic Sensing, University of Duisburg-Essen. His current research interests are in the area of antennas and RF technologies, UWB antennas, and chipless RFID tags.

ALEJANDRO JIMÉNEZ-SÁEZ (Member, IEEE) was born in Valencia, Spain. He received the master's degree in telecommunications engineering from the Polytechnic University of Valencia, Spain, in 2017, and the master's degree in electrical engineering from the Technische Universität Darmstadt, Germany, in 2017, where he is currently pursuing the Ph.D. degree with the Institute of Microwave Engineering and Photonics. His current research interests include chipless RFID, high-Q resonators, and electromagnetic bandgap structures in microwave and mm-wave frequencies.

AYA MOSTAFA AHMAD received the B.Sc. and M.Sc. degrees in electrical engineering from the German University in Cairo, Egypt, in 2011 and 2014, respectively. She is currently pursuing the Ph.D. degree with the Institute of Digital Communication Systems, Ruhr-Universität Bochum, Germany. Her research interests include MIMO radar signal processing, waveform design optimization, cognitive radars, direction of arrival algorithms, and machine learning applications for radar resources management.

MARTIN SCHÜßLER (Member, IEEE) received the Dipl.-Ing. and Ph.D. degrees from the Technische Universität Darmstadt, Darmstadt, Germany, in 1992 and 1998, respectively. Since 1998, he has been a Staff Member with the Institute of Microwave Engineering and Photonics, Technische Universität Darmstadt. He was involved in III–V semiconductor technology, microwave sensors for industrial applications, RFID, and small antennas. His current research interest includes the application of metamaterials for industrial and biomedical sensing.

ANDREAS RENNINGS (Member, IEEE) received the degree in electrical engineering and the Dipl.-Ing. and Dr.-Ing. degrees from the University of Duisburg-Essen, Germany, in 2000 and 2008, respectively. He carried out his diploma work during a stay at the University of California at Los Angeles. From 2006 to 2008, he was with IMST GmbH, Kamp-Lintfort, Germany, where he was an RF engineer. Since 2008, he has been a Senior Scientist and a Principal Investigator with the Laboratory for General and Theoretical Electrical Engineering, University of Duisburg-Essen. His general research interests include all aspects of theoretical and applied electromagnetics, with an emphasis on medical applications and on-chip millimeter-wave/THz antennas. He received several awards, including a Student Paper Award at the 2005 IEEE Antennas and Propagation Society International Symposium and the VDE-Promotionspreis 2009 for the dissertation.

KLAUS SOLBACH (Member, IEEE) was with the University of Duisburg-Essen as a Junior Researcher in the field of integrated dielectric image line circuits from 1975 to 1980. In 1981, he joined the Millimeterwave Research Laboratory, AEG-Telefunken, Ulm, and in 1984, he moved to the Radar Systems Group, Daimler-Benz Aerospace (currently a part of Airbus Group), where he was involved in the design and production of microwave-subsystems for ground-based and airborne Radar, EW, and communication systems, including phased-array and active phased-array antenna systems. His last position was the Manager of the Department of RF-and-Antenna Subsystems. In 1997, he joined the Faculty of the University of Duisburg-Essen as the Chair of RF and microwave technology. He has authored and coauthored over 200 national and international articles, conference contributions, book chapters, and patent applications. He was the Chairman of the VDE-ITG Fachausschuss Antennen, an Executive Secretary of the Institut für Mikrowellen-und Antennentechnik, and the Chair of the IEEE Germany AP/MTT Joint Chapter. He was the General Chair of the International ITG-Conference on Antennas INICA2007, Munich, and the European Conference on Antennas and Propagation EuCAP2009, Berlin.

THOMAS KAISER (Senior Member, IEEE) received the Diploma degree in electrical engineering from Ruhr-Universität Bochum, Bochum, Germany, in 1991, and the Ph.D. (Hons.) and German Habilitation degrees in electrical engineering from Gerhard Mercator University, Duisburg, Germany, in 1995 and 2000, respectively. From 1995 to 1996, he spent a research leave with the University of Southern California, Los Angeles, which was grant-aided by the German Academic Exchange Service. From 2000 to 2001, he was the Head of the Department of Communication Systems, Gerhard Mercator University, and from 2001 to 2002, he was the Head of the Department of Wireless Chips and Systems, Fraunhofer Institute of Microelectronic Circuits and Systems, Duisburg. From 2002 to 2006, he was a Co-Leader of the Smart Antenna Research Team, University of Duisburg-Essen, Duisburg. In 2005, he joined the Smart Antenna Research Group, Stanford University, Stanford, CA, USA, as a Visiting Professor, and in 2007, he joined the Department of Electrical Engineering, Princeton University, Princeton, NJ, USA, as a Visiting Professor. From 2006 to 2011, he headed the Institute of Communication Technology, Leibniz University of Hannover, Germany. He is currently the Head of the Institute of Digital Signal Processing, University of Duisburg-Essen, and also the Founder and the CEO of ID4us GmbH, an RFID centric company. He has authored and coauthored over 300 articles in international journals and conference proceedings and two books *Ultra Wideband Systems with MIMO* (Wiley, 2010) and *Digital Signal Processing for RFID* (Wiley, 2015). He was the Founding Editor-in-Chief of the e-letter of the IEEE Signal Processing Society and the General Chair of the IEEE International Conference on Ultra WideBand in 2008, the International Conference on Cognitive Radio Oriented Wireless Networks and Communications in 2009, the IEEE Workshop on Cellular Cognitive Systems in 2014, and the IEEE Workshop on Mobile THz Systems in 2018. He is the Speaker of the Collaborative Research Center Mobile Material Characterization and Localization by Electromagnetic Sensing.

ROLF JAKOBY (Member, IEEE) was born in Kinheim, Germany, in 1958. He received the Dipl.-Ing. and Dr.-Ing. degrees in electrical engineering from the University of Siegen, Germany, in 1985 and 1990, respectively. In 1991, he joined the Research Center of Deutsche Telekom, Darmstadt, Germany. Since 1997, he has been a Full Professor with Technische Universität Darmstadt, Germany. He is a Co-Founder of ALCAN Systems GmbH. He has authored more than 320 publications. He holds more than 20 patents. His research interests include chipless RFID sensor tags, biomedical sensors and applicators, tunable passive microwave/millimeter wave devices, and beam-steering antennas, using primarily ferroelectric and liquidcrystal technologies. He is also a member of VDE/ITG and IEEE/MTT/AP societies. He received the award from CCI Siegen for his excellent Ph.D. in 1992 and the ITG-Prize for an excellent publication in the IEEE TRANSACTIONS ON ANTENNAS AND PROPAGATION in 1997. His group received 23 awards and prizes for best articles and doctoral dissertations. He is also the Editor-in-Chief of *FREQUENZ* and *DeGruyter*. He was the Chairman of the EuMC in 2007 and the GeMiC in 2011, and the Treasurer of the EuMW in 2013 and 2017, respectively.

AYDIN SEZGIN (Senior Member, IEEE) received the Dipl.-Ing. (M.S.) degree in communications engineering from Technische Fachhochschule Berlin, Berlin, in 2000, and the Dr.-Ing. (Ph.D.) degree in electrical engineering from the Berlin Institute of Technology in 2005. From 2001 to 2006, he was with the Heinrich-Hertz-Institut, Berlin. From 2006 to 2008, he held a postdoctoral position and also a Lecturer with the Information Systems Laboratory, Department of Electrical Engineering, Stanford University, Stanford, CA, USA. From 2008 to 2009, he held a postdoctoral position with the Department of Electrical Engineering and Computer Science, University of California at Irvine, Irvine, CA, USA. From 2009 to 2011, he was the Head of the Emmy-Noether Research Group on Wireless Networks, Ulm University. In 2011, he joined Technische Universität Darmstadt, Germany, as a Professor. He is currently a Professor of information systems and sciences with the Department of Electrical Engineering and Information Technology, Ruhr-Universität Bochum, Germany. His research interests include in signal processing, communication, and information theory, with an emphasis on wireless networks. He has published several book chapters more than 40 journals and 140 conference papers in these topics. He has coauthored a book on multiway communications. He was a recipient of the ITG-Sponsorship Award in 2006. He was a first recipient of the prestigious Emmy-Noether Grant at the German Research Foundation in communication engineering in 2009. He has coauthored articles that received the Best Poster Award at the IEEE Communication Theory Workshop in 2011, the Best Paper Award at ICCSPA in 2015, and the Best Paper Award at ICC in 2019. He has served as an Associate Editor for the IEEE TRANSACTIONS ON WIRELESS COMMUNICATIONS, from 2009 to 2014.

DANIEL ERNI (Member, IEEE) received the Diploma degree in electrical engineering from the University of Applied Sciences Rapperswil in 1986, and the Diploma degree in electrical engineering and the Ph.D. degree in laser physics from ETH Zurich in 1990 and 1996, respectively. Since 1990, he has been with the Laboratory for Electromagnetic Fields and Microwave Electronics, ETH Zurich. From 1995 to 2006, he has been the Founder and the Head of the Communication Photonics Group, ETH Zurich. Since 2006, he has been a Full Professor of general and theoretical electrical engineering with the University of Duisburg-Essen, Germany. In 2017 and 2018, he was a Visiting Professor with the Institute of Electromagnetic Fields, ETH Zürich. He is a Co-Founder of airCode, a spin-off company on flexible printed RFID technology. His current research interests include optical interconnects, nanophotonics, plasmonics, advanced solar cell concepts, optical and electromagnetic metamaterials, RF, mm-wave and THz engineering, biomedical engineering, bioelectromagnetics, marine electromagnetics, computational electromagnetics, multiscale and multiphysics modeling, numerical structural optimization, and science and technology studies. He is a Fellow of the Electromagnetics Academy, a member of the Center for Nanointegration Duisburg-Essen, the Swiss Physical Society, the German Physical Society, and the Optical Society of America.